

Oxidation kinetics of copper at reduced oxygen partial pressures

Matts Björck
SKB

Ragna Elger
Swerea KIMAB

Oct, 2013

Sammanfattning

I denna studie undersöks oxidationshastigheten för koppar med experiment och matematisk modellering. Experimenten är utförda i termovåg vid olika syrepartialtryck ($100 \text{ ppm} < p_{\text{O}_2} < 21\%$) och vid temperaturer relevanta för svetsprocessen ($270^\circ\text{C} < T < 900^\circ\text{C}$). Data från den experimentella delen har sedan använts i en matematisk modell.

Resultatet är en modell som kan förutsäga oxidationshastigheten inom ovan angivna temperaturer och syrehalter. Modellen visar att oxidationsförloppet kan beskrivas med en linjär och en parabolisk term, där den linjära termen dominerar vid låga temperaturer och låga syrepartialtryck, medan den paraboliska termen är viktigare vid höga temperaturer och högre syrepartialtryck. Modellens giltighet utanför experimentområdet diskuteras även.

Summary

This study examines the oxidation kinetics of copper. The experiments were performed in a thermobalance at various partial pressures of oxygen ($100 \text{ ppm} < p_{\text{O}_2} < 21\%$) at different temperatures relevant for the welding process ($270^\circ\text{C} < T < 900^\circ\text{C}$). The results from the experimental part were then used to model the process.

The result is a model able to predict the oxidation rate of copper at the partial pressures and temperatures relevant for the welding process. The model describes kinetics up to 8 h as a combination of linear and parabolic behaviour, where the first linear part is dominating at low partial pressures, whereas the parabolic term is dominant at higher partial pressures of oxygen. The applicability of the model outside the validated interval is also discussed.

Table of contents

1	Introduction	4
2	Oxidation kinetics of copper	5
2.1	High temperature oxidation	5
2.2	Low temperature oxidation.....	5
2.3	Effect of oxygen pressure	6
2.4	Evaluation of previous data	6
2.5	Conclusions from previous work.....	8
3	Experimental details.....	9
4	Results and discussion.....	11
4.1	Exposures at 270°C, varying p_{O_2}	11
4.2	Exposures at 900°C, varying p_{O_2}	11
4.3	Exposures in 1000 ppm O_2 /Ar at different temperatures.....	14
4.4	Exposures in Ar/1.8 mol-% H_2 /1000 mol-ppm O_2	15
4.5	Modelling	16
5	Conclusions	20
	References	21
	Appendix 1	23
	Appendix 2	24

1 Introduction

The spent nuclear fuel produced from nuclear power reactors in Sweden are proposed to be deposited in a final repository following the KBS-3 concept. The fuel elements will be placed in a load-bearing cast iron insert which is surrounded by a copper canister that functions as a corrosion barrier. The canister is surrounded by bentonite clay which serves as a diffusion barrier as well as protecting the canister from rock movements. The repository will be located at a depth of about 500 m in the Swedish basement rock. The system must contain the fuel for 100 000 years, which puts stringent demands on the components.

A critical step in the assembly of the copper canister is the sealing. The reference technique for sealing the canisters is a solid state welding technique called Friction Stir Welding (FSW). A brief description can be found in SKB (2010). The reliability of FSW with regards to produced defects and non destructive testing has been evaluated (Ronneteg et al. 2006). The welds produced by FSW have creep properties close to the parent material (Andersson-Östling and Sandström 2009) as well as suitable corrosion properties (Gubner and Andersson 2007).

During the last decade questions have arisen of the effect of oxide particles that forms during welding. In one study (Savolainen 2012) it has been seen that the material ruptures at or near the processing line where the oxides particles have their highest concentration. This is in contradiction to a previous study which indicated that the heat affected zone outside the weld area was the location of rupture (Andersson et al. 2007). There has also been seen oxidation in root defects in some of the first welds produced (Auerkari et al. 2012). This defect caused a reduction in creep life and ductility compared to the parent material. To increase the understanding and reduce the amount of oxide particles in the weld a development program has been started at SKB.

To set a limit on the oxygen content at the joint line during welding as well as to achieve a more quantitative understanding of the oxidation formation process a literature study was conducted regarding the oxidation of copper, see section 2. This revealed that although the oxidation kinetics of copper is a well studied area the oxidation kinetics below an oxygen partial pressure of 0.1 % in an inert gas atmosphere is still not fully mapped out. The lower range of oxygen pressure is interesting as a large change in the oxidation rate is expected, providing an avenue to reduce the amount of oxides formed during welding. Therefore, more experimental work was deemed necessary to develop a model that estimated the amount of oxide forming under conditions relevant to FSW conducted under inert gas atmospheres with an oxygen content below 0.1% at a temperature range relevant to the FSW process. The temperature range of FSW welding of copper canisters has been measured in “FSWL94 – Measurement of temperatures and surrounding oxygen levels during welding” (SKBdoc 1371191) to extend from room temperature to about 900°C. As an alternative a reducing atmosphere, which destabilizes the stability of copper oxides, is included in the study for comparison.

2 Oxidation kinetics of copper

This section gives a brief background to the literature of the oxidation kinetics of copper. It is not intended as a full review of the field as the research extends from the first half of the 20th century up to today. Instead, reviews and literature of direct interest are presented. Since the aim is to mathematically describe oxidation rates the exact physical mechanisms are of lesser importance but are briefly commented upon when deemed necessary.

Copper forms two different oxides; cuprous oxide, Cu_2O , and cupric oxide, CuO . Which oxide that forms during oxidation depends on the temperature as well as the oxygen pressure (Kofstad 1988, Zhu et al. 2006). Under the conditions expected for welding with an oxygen partial pressure below 21% cupric oxide is expected to be the dominating reaction product (Zhu et al. 2006).

2.1 High temperature oxidation

High temperature oxidation was recently reviewed by Zhu et al. (Zhu et al. 2006) and the early literature were included in the review by Rönnqvist and Fischmeister (1961). A majority of the reviewed literature in the high to medium temperature regime (Rönnqvist and Fischmeister 1961, Zhu et al. 2006) showed that the weight gain, x , as a function of time, t , above 100 – 200 °C followed a parabolic rate law

$$x^2 = k_p t + C, \quad (2-1)$$

where k_p is the parabolic rate constant and C is a constant which accounts for any oxidation prior to $t = 0$.

The parabolic rate law arise when a diffusive process through the oxide is the rate limiting process, for a review see Cabrera and Mott (1949). In the case of copper the rate limiting step is outward diffusion of metal ions through the oxide layer. Initially, accelerated oxidation will occur before the diffusive barrier is created (Cabrera and Mott 1949). However, this is in general not seen at elevated temperatures due to the rate of oxidation and will be detailed below for low temperature oxidation.

2.2 Low temperature oxidation

The data reviewed by Rönnqvist and Fishmeister (1961) showed that at temperatures below 100-200°C oxidation proceeds with other rate laws. Various rate laws were observed, for example inverse logarithmic or logarithmic laws. Newer studies showed that the parabolic regime continues down to 100°C (Roy et al. 1990, Pinnel et al. 1979). Pinnel et al.'s data showed that at temperatures of 50°C and 75°C an oxide of a thickness of 1 nm was established within the first 4 h of exposure. After this initial oxidation the growth slowed down during the remainder of the experiment, which lasted 42 days. The total film thickness was below 2 nm. Similar results, oxide thickness below 5 nm for oxidations times lasting 4.5 days, were reported by Krishnamoorthy and Sircar (1970). That data could be represented with a differential form of an inverse logarithmic equation. Roy et al. (1991) found that the oxidation could be represented by a logarithmic rate law in the temperature range of 75 – 100°C. The maximum film thickness achieved after 3 h was 12 nm, an order of magnitude larger than Pinnel et al. (1979).

At room temperature an initial oxide layer forms rapidly. After half an hour an oxide thickness of about 1 nm formed on high purity surfaces (Suzuki 1997). The growth speed after this initial oxidation is slow and the same study shows that after 11 days the oxide grew to a thickness of about 4.5 nm. Similar trends were seen for ion beam deposited films (Iijama 2006), however an increase in oxidation was seen after 13-33 days when the oxidation rate accelerated. The initial rapid growth can be qualitatively explained by an initial growth of oxide islands and when the islands coalesce the oxidation is slowed down (Yang et al. 1998).

To conclude, it can be expected that a clean copper surface rapidly acquires an oxide of a thickness of about 1 nm. This order of magnitude of the oxide thickness will be maintained for an extended period, at least several days. However, it is known that different pollutants can affect the atmospheric corrosion rates of copper (Rice et al. 1981). If the temperature is above 100 °C a parabolic rate law is expected to describe the oxidation process.

2.3 Effect of oxygen pressure

Although the temperature dependence of the oxidation rate has been well studied the dependence on the oxygen content has not received the same attention. Two studies (Roy et al. 1991, Mrowec and Stokłosa 1971) focused on oxygen partial pressures, p_{O_2} , in the range of 100 – 2.1×10^4 Pa. At these conditions a parabolic rate law was identified and the dependence on the oxygen content followed a $k_p \propto p_{O_2}^{1/7}$ or $k_p \propto p_{O_2}^{1/4}$, not in agreement with each other. Different exponents could be theoretically explained by differently charged vacancies in the growing film (Roy et al. 1991). These vacancies allow the copper atoms to diffuse to the surface.

Another study (Ogbuji and Humphrey 2003) going to even lower oxygen partial pressures, $p_{O_2} = 33$ Pa revealed a linear behaviour. The same observation was done with ellipsometry at a pressure of $5 \cdot 10^{-6} atm$ (Rauh and Wißmann 1993). The parabolic to linear transition were described by Wagner and Grünewald (1938) as well as Rönqvist and Fischmeister (1961). The rate equation was written as

$$\frac{x}{k_l} + \frac{x^2}{k_p} = t, \quad (2-2)$$

where k_l is the linear rate constant. The believed mechanism behind the linear kinetics was a reaction at the Cu_2O/O_2 interface which competed with the diffusion through the oxide layer. For the parabolic part Wagner and Grünewald (1938) observed a $k_p \propto p_{O_2}^{1/7}$ behaviour. The same form of rate equation was derived to describe the thermal oxidation of Si to SiO_2 (Deal and Grove 1965).

2.4 Evaluation of previous data

The k_p values from several different studies¹ have been summarized in Figure 2-1. The low temperature data (Roy et al. 1991, Pinnel et al. 1979) were given in thickness rates rather than weight rates. These data were recalculated to thickness rates with the transformation $1 \mu g/cm^2 = 14.65 nm$ calculated from the atomic densities of Cu_2O . As can be seen from the figure the high temperature data shows good agreement. Below 500°C a larger spread between studies appears. The maximum spread amounts to two orders of magnitude at 350°C. To mathematically model the temperature behaviour a double Arrhenius expression was used

$$k_p(T) = A_1 e^{-\frac{E_1}{RT}} + A_2 e^{-\frac{E_2}{RT}}, \quad (2-3)$$

where A_1 and A_2 are amplitude factors. E_1 , E_2 are activation energies. The two term expression can be explained by a combination of lattice diffusion at high temperatures and grain boundary diffusion at low temperatures. Assuming that the two processes have two separate channels of diffusion and that the fraction of grain boundaries is constant with time and temperature yields a linear expression as above (Zhu et al. 2006). The resulting least square fit, achieved by varying the four parameters, can be seen as a dashed line in Figure 2-1. The resulting fitting parameters are presented in Table 2-1. From the figure it can be seen that term 1 is only needed for the

¹ As Zhu et al. (2006) showed that the purity content had an effect of the oxidation rate, high purity, above 4N, has been excluded from the data used in Figure 2-1.

modelling of temperatures above 800 °C. The activation energies in Table 2-1 is in the same range as most of the literature values reviewed by Zhu (2006). Adding a third term did not improve the agreement between the model and the current data. A two term expression provided a better fit than a single Arrhenius expression.

Table 2-1. The values of the fitted parameters for the Arrhenius expression used to model the parabolic rate constant.

Parameter	Fitted value
A_1	$634 \text{ g}^2/(\text{cm}^4\text{s})$
A_2	$8.67 \cdot 10^{-4} \text{ g}^2/(\text{cm}^4\text{s})$
E_1	248 kJ/mol
E_2	103 kJ/mol

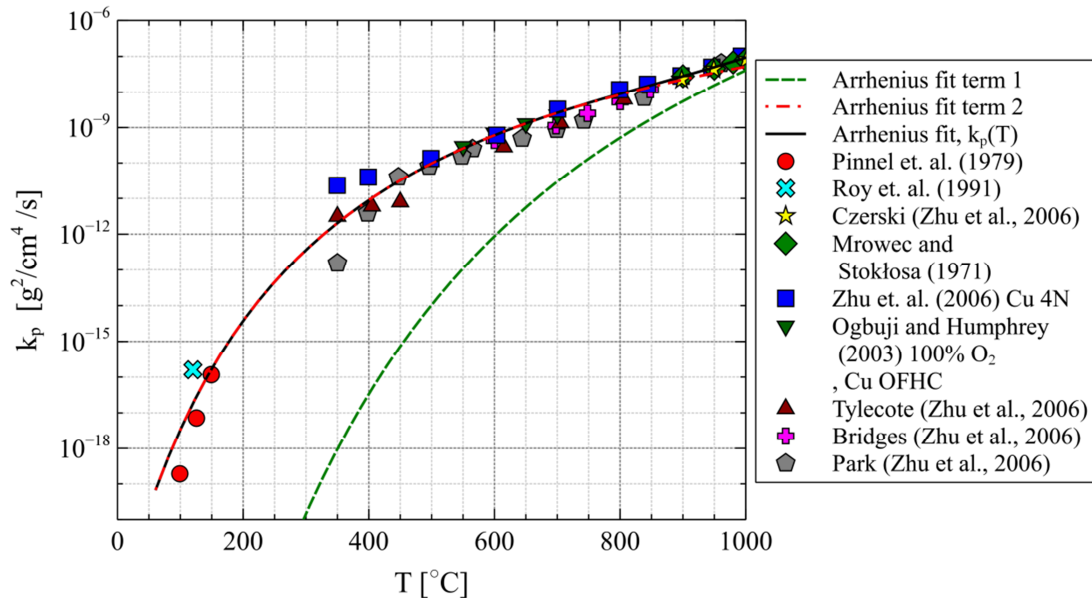


Figure 2-1. The temperature dependence of k_p . The entire temperature range can be described by a linear combination of two Arrhenius expressions (full line). The legend denotes the data sources. The inset shows the high temperature region with a linear y-axis which emphasise the necessity of the first Arrhenius term to describe the data.

To compare the different data from varying oxygen partial pressures the $k_p(p_{O_2}, T)$ values from the literature were normalized with the fitted, equation (2-3), value for the same temperature. The result can be seen in Figure 2-2. The dependence of k_p on p_{O_2} is weak, the value of k_p varies little compared to the temperature dependence. The low temperature data reported by Roy et al. (1991) deviates significantly from the rest of the data. This is due to the fact that the fitted expression, see Figure 2-2, deviate one order of magnitude from the data point at atmospheric conditions.

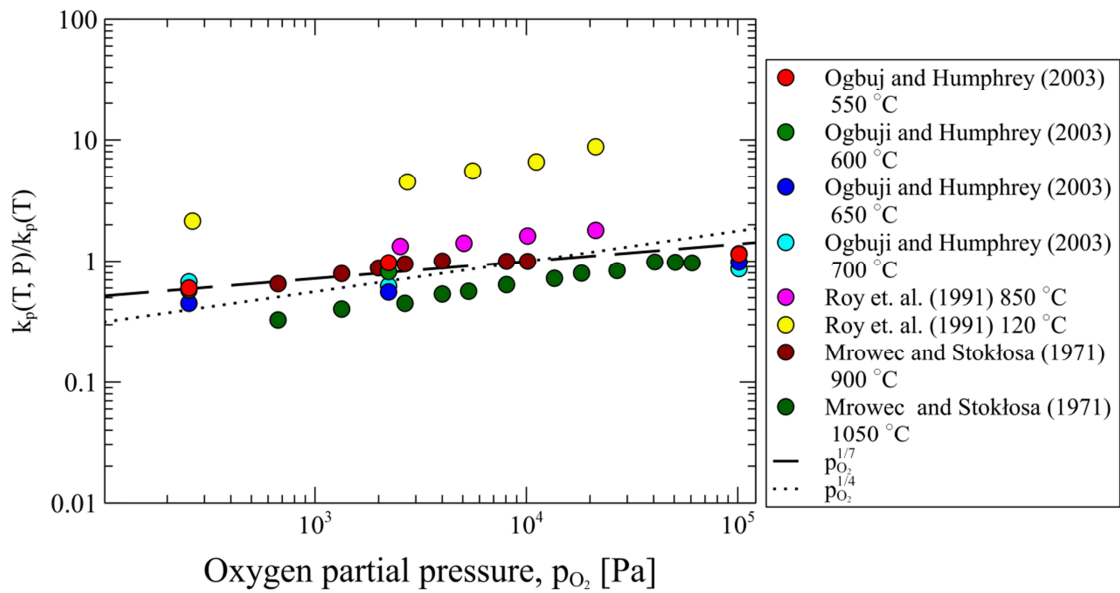


Figure 2-2. The pressure dependence of k_p normalized with the fitted expression. The legend gives reference to the source of the data points. Also included are the previously proposed pressure dependencies as lines.

2.5 Conclusions from previous work

As detailed above, the oxidation kinetics under atmospheric conditions has been well studied and need very little further study. The linear combination of two Arrhenius rate laws yielded a mathematical representation that deviate at most one order of magnitude from any of the reviewed data.

Although the data in the literature is rather consistent for oxygen partial pressures in the range $10^2 - 10^5$ Pa the kinetics for $p_{O_2} \leq 10^2$ Pa is still an open question concerning the rate constants. A rate equation, eq. (2-2), has been proposed but the linear rate constant's, k_l , temperature or pressure dependence have not been determined. However, k_l drops faster with reducing oxygen content than k_p (Wagner and Grünewald 1938).

To conclude, it is necessary to investigate the pressure dependence and temperature dependence in or close to the linear region where the oxidation rate decrease faster with p_{O_2} . This part is also of interest for the FSW process due to the reduced oxidation rate. The temperature dependence of k_l has to be explored as well since the linear kinetics has a different physical origin than the parabolic rate constant.

3 Experimental details

The exposures were performed using thermo gravimetric analysis (TGA) in an equipment from Rubotherm (mass measuring accuracy ± 0.02 mg) with both test and protection gas entering at the top of the equipment and leaving at the bottom. A TGA test curve was run using Ar with equal conditions as the exposures for the empty crucible (blank sample) at every temperature used in the study. The mass gain recorded for this blank sample was then subtracted from the test curve to give the result.

Before every exposure, the oven was flushed for at least 3 h with Ar. Typical oxygen levels after 3 h corresponded to a range 30-45 ppm O₂ vol/vol. After the initial flushing, heating to test temperature was conducted in Ar 60 mL/min + 5 mL Ar/min protection gas. After temperature stabilisation for 10 min at specified temperature, the gas through the main gas entrance was switched from Ar to test gas according to the test plan (Table 3-1). Time of exposure was set to 8 h with subsequent cooling to room temperature in test gas. All measurements were conducted at ambient pressures. The actual concentration of the test gases are given in Table 3-2.

Table 3-1. Test plan for exposures performed within the study

Test gas	O ₂ partial pressure [Pa]	270°C	500°C	700°C	900°C	900°C, 120+5 mL/min
Ar/21 mol% O ₂	2.1×10^4	1A			1B	
Ar/1 mol% O ₂	1×10^3	2A			2B	
Ar/1000 mol-ppm O ₂	100	3A	3D	3E	3B	3C
Ar/100 mol-ppm O ₂	10	4A			4B	
90% (Ar/2% H ₂)-10% (Ar/1% O ₂)	100	5A			5B	

Table 3-2. Premixed gases used within the study

Test gas	Concentration of O ₂ according to analysis	Analytical tolerance
Ar/1% O ₂	0.997 mol-%	$\pm 1\%$
Ar/1000 ppm O ₂	986 mol-ppm	$\pm 1\%$
Ar/100 ppm O ₂	98.5 mol-ppm	$\pm 2\%$
Ar/2% H ₂	1.96 mol-%	$\pm 2\%$

In order to keep the surfaces as close as possible to the joint surfaces the samples was exposed after they had been dry-milled without any cutting fluids. They were handled using tweezers to avoid any unwanted contamination. No measurements of the geometrical dimensions were performed, the nominal surface area of $5.22 \pm 0.07 \text{ cm}^2$ has been used in all calculations. To complete the measurements, the weights of most samples were also determined using a separate balance (Sartorius BP 2110) with measuring accuracy of ± 0.06 mg. Before exposure, the sample and the crucible were weighed separately. After exposure, the total weight of crucible and sample was determined, then sample and crucible were weighed separately. Before the weighing, the samples were left in the same room as the balance to attain the temperature of the room for at least 20 min.

After exposures at 900°C, most samples displayed spallation and some contamination by copper in the crucible used for the exposures was observed. To avoid erroneous results from oxidation tests, the crucible was put into an oxidising atmosphere at 1000°C for 24 h before next exposure. As the metal/metal oxide of the crucible was then completely oxidised, additional mass gain due to oxidation of remaining oxide of the crucible was minimised.

Before exposures in the mixture of (1 mol-% O₂/Ar + Ar/2 mol-% H₂), the remaining metal/metal oxide of the crucible was instead reduced for 24 h at 1000°C in Ar/2 mol-% H₂ to avoid weight reduction of oxide that would conceal any weight increase during exposure.

4 Results and discussion

4.1 Exposures at 270°C, varying p_{O_2}

After exposures at 270°C, the oxide layers were thin at all examined partial pressures of oxygen. Photographs of exposed samples at $p_{O_2} = 10 \text{ Pa}$ (100 ppm O_2) and $p_{O_2} = 100 \text{ Pa}$ (1000 ppm O_2) are shown in Figure 4-1. The measured weight gain was small and is given in Table 4-1 for all samples.

Table 4-1. Results from mass measurements before and after exposures at 270°C. In the table, the mass of the sample before exposure, the total weight of the sample and crucible before exposure and the total weight after exposure is shown. The accuracy of the mass measurements are 60 μg .

Exposure	Mass of sample before exposure (g)	Total mass before exposure (g)	Total mass after exposure (g)	Mass gain (μg)
Ar/21% O_2	4.8236	8.8664	8.8668	373
Ar/1% O_2	4.8619	8.9083	8.9086	310
Ar/1000 ppm O_2	4.8757	8.9190	8.9193	293
Ar/100 ppm O_2	4.8709	8.9200	8.9202	140

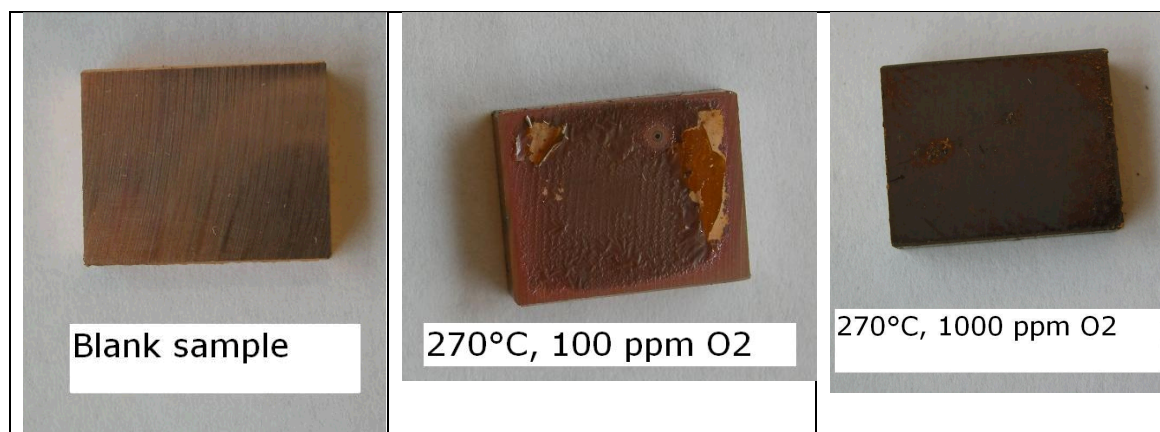


Figure 4-1. Photographs of an unexposed sample and samples exposed at 270°C in environments with 100 ppm ($p_{O_2} = 10 \text{ Pa}$) or 1000 ppm O_2 ($p_{O_2} = 100 \text{ Pa}$) in Ar.

4.2 Exposures at 900°C, varying p_{O_2}

After exposures at 900°C, the oxide layer was thick and spallation was evident on most samples. Spallation had occurred in large flakes. As mass gain data from the thermogravimetric exposures are smooth and spall in the crucible were found to be large flakes, it is assumed that spallation have occurred upon cooling. Spallation of large flakes during exposure would be followed by an increased oxidation rate due to access to fresh metal surface. Also, initial measurements using glow discharge spectroscopy on oxidised samples exposed at 800°C displayed consistency between measured oxide thickness and oxide thickness calculated from mass gain data. Spallation upon cooling occurs due to the different coefficients of thermal expansion between the metal and oxide and is often observed after high temperature exposures. However, spallation during exposure cannot be excluded since samples were exposed in a crucible and any spall is collected within the crucible. Mass data from the balance is given in Table 4-2 below, whereas thermogravimetric data are given in Figure 4-2 and photographs of some samples are given in Figure 4-3. As can be seen in Figure 4-2 the oxidation comes to a halt as soon as the temperature is lowered although the sample is still exposed to the test gas. This is primarily due to the sharp initial decay of the temperature which rapidly changes the rate

constant, compare to Figure 2-1. Also, an oxide scale is formed at high temperatures on the samples which will slow down the oxidation rate at the lower temperatures if the rate limiting step is diffusion controlled (see section 2.3).

Table 4-2. Results from mass measurements before and after exposures at 900°C. In the table, mass of the samples before exposure, total weight of sample and crucible before exposure and total weight after exposure are given. Note that data for mass gain of the exposure performed in 21% O₂ originates from the TGA equipment and not from measurements using a separate balance as the remaining measurements. The accuracy of the mass measurements are 60 µg.

Exposure	Mass of sample before exposure (g)	Total mass of sample and crucible before exposure (g)	Total mass of sample and crucible after exposure (g)	Mass gain (mg)
Ar/21% O ₂	n/a	n/a	n/a	137.02
Ar/1% O ₂	4.8066	8.8500	8.9526	102.66
Ar/1000 ppm O ₂ 3B	4.8876	8.9304	8.9490	18.61
Ar/1000 ppm O ₂ 3C	4.7813	8.8278	8.8505	22.74
Ar/100 ppm O ₂	4.8660	8.9154	8.9172	1.86

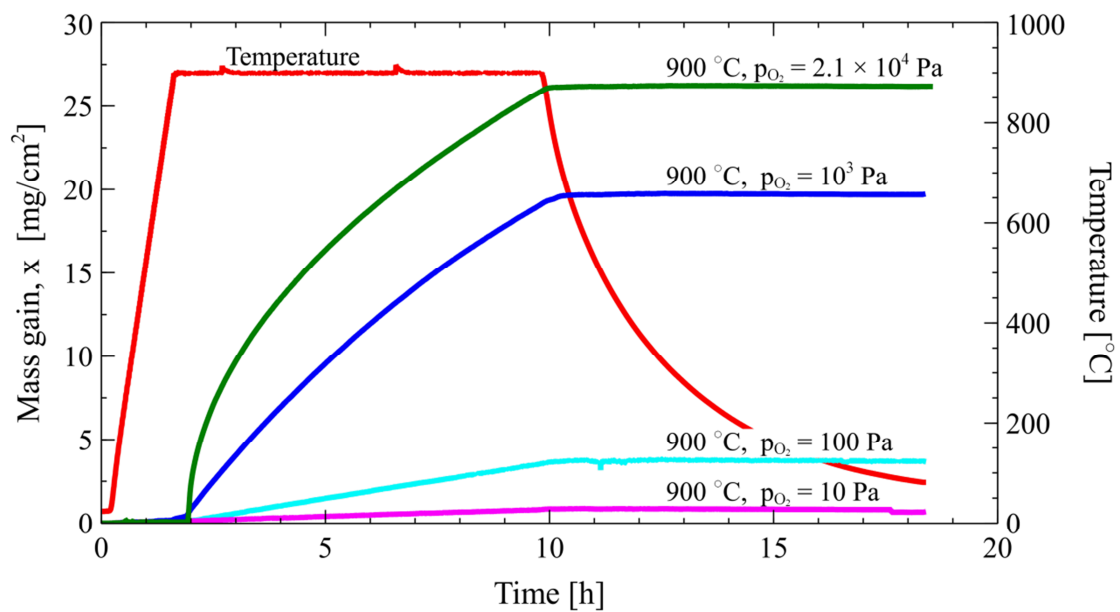


Figure 4-2. Mass gain per unit area as function of exposure time at different oxygen partial pressures at a total gas flow of 60mL test gas/min at a temperature 900°C.

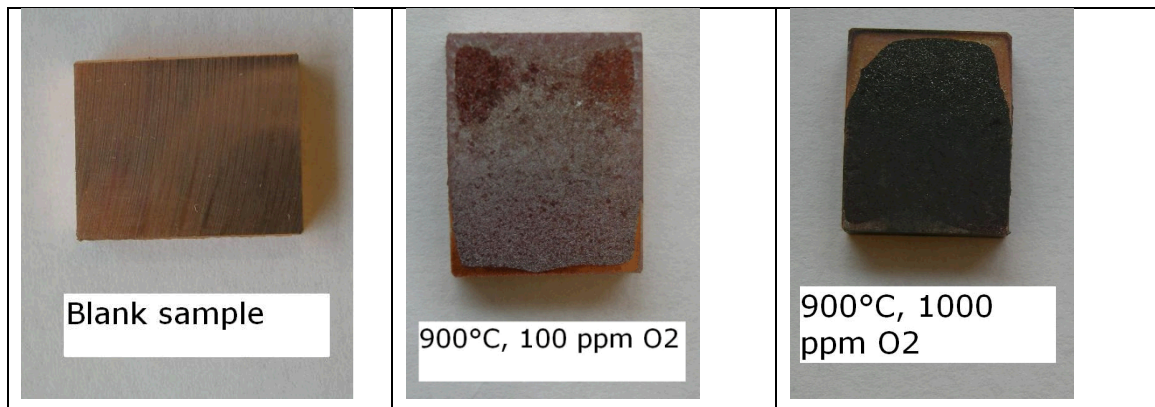


Figure 4-3. Photographs of an unexposed sample and samples exposed at 900°C in environments with 100 ppm ($p_{O_2} = 10 \text{ Pa}$) or 1000 ppm O_2 ($p_{O_2} = 100 \text{ Pa}$) in Ar.

As observed, the oxidation rate of sample 3B was linear. To examine if this behaviour was only an effect of limited oxygen supply, another exposure with $p_{O_2} = 100 \text{ Pa}$ but with doubled flow of test gas was conducted (exposure 3 C). The reaction rate in this exposure was found to be linear as well. Total mass gains from the two exposures 3B and 3C were in the same range (Table 4-2) and thermogravimetric data show linear behaviour for both exposures. It was assumed that the oxidation behaviour rather than the limited supply of oxygen was the reason for the linear behaviour at this exposure time span. Also after exposure with $p_{O_2} = 10 \text{ Pa}$, mass gain was observed to increase linearly with time.

If data for exposures with $p_{O_2} = 10^3 \text{ Pa}$ and $p_{O_2} = 2.1 \times 10^4 \text{ Pa}$ are plotted as the square of mass gain versus time, see Figure 4-4, it is observed that the exposure with $p_{O_2} = 2.1 \times 10^4 \text{ Pa}$ exhibits parabolic behaviour as soon as the sample is exposed to the active gas, while the exposure of $p_{O_2} = 10^3 \text{ Pa}$ results in a parabolic behaviour after an initial period of linear behaviour as shown in Figure 4-4. Parabolic constants for $p_{O_2} = 2.1 \times 10^4 \text{ Pa}$ and $p_{O_2} = 10^3 \text{ Pa}$ were calculated to be $2.4 \cdot 10^{-8} \text{ g}^2 \cdot \text{cm}^{-4} \cdot \text{s}^{-1}$ and $1.6 \cdot 10^{-8} \text{ g}^2 \cdot \text{cm}^{-4} \cdot \text{s}^{-1}$ respectively, which is in good agreement, although somewhat lower than the literature value (Kofstad 1988, pp 186–189). The calculated rate constant for $p_{O_2} = 2.1 \times 10^4 \text{ Pa}$ is compared to the previously analysed literature data (see Figure 2-1) in Figure 4-5. The experiments in this study do not deviate more from the fitted Arrhenius expression than the found literature data. This shows that although the surfaces of the samples were in as-milled conditions this did not cause an increased deviation as compared to the values in the literature in the parabolic regime.

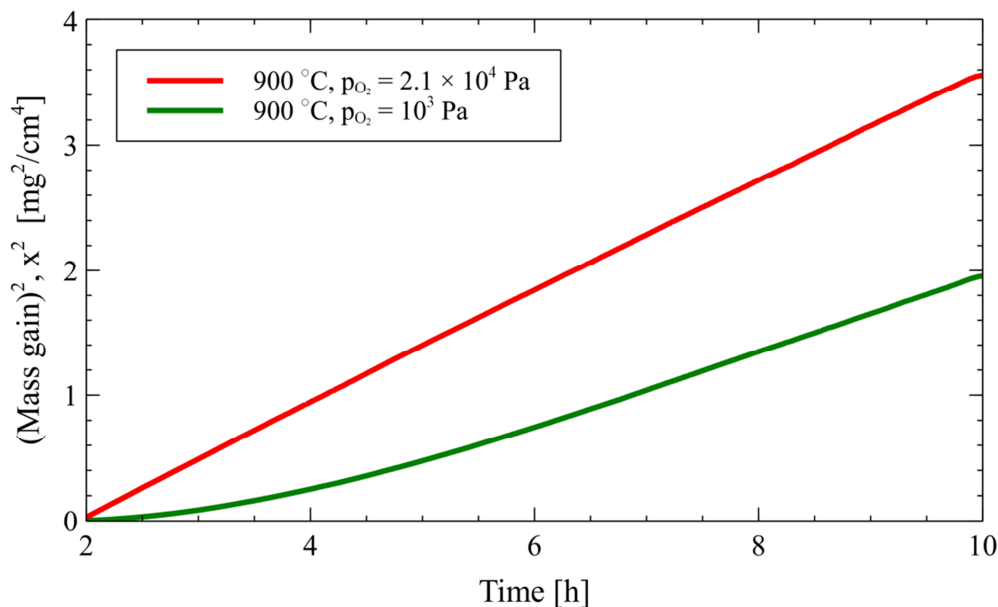


Figure 4-4. Square of mass gain plotted versus time for exposures at 900°C in 1% and 21% O₂ respectively.

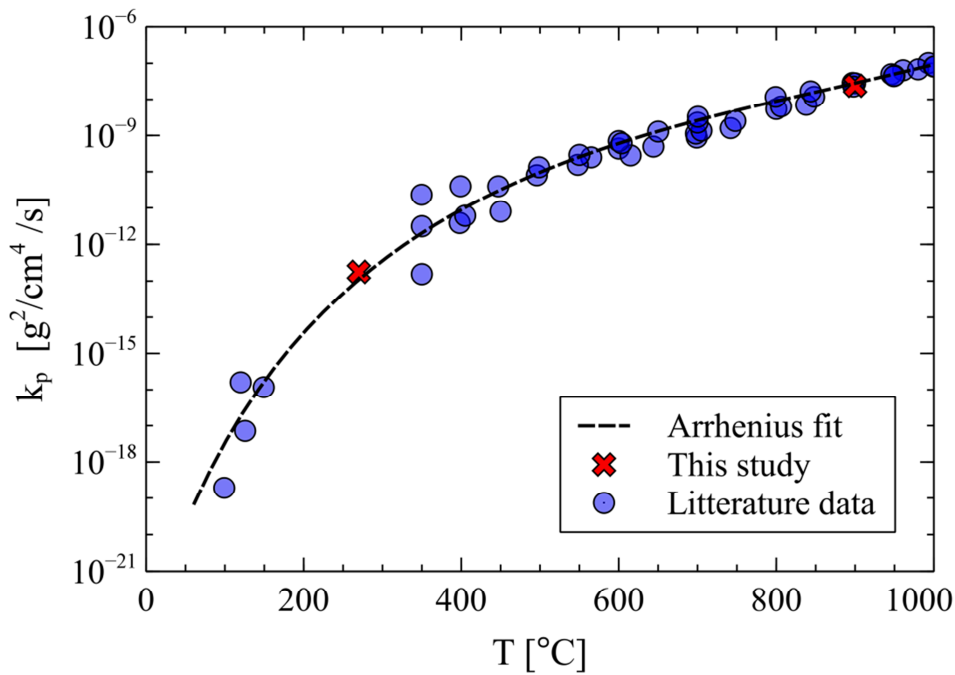


Figure 4-5. Experimental data, crosses, obtained in this study compared with data taken from the literature, circles. The literature data is the same as for Figure 2-1.

4.3 Exposures in 1000 ppm O₂/Ar at different temperatures

After exposures with $p_{O_2} = 100$ Pa at different temperatures, a linear behaviour was observed at both 900°C and 700°C, as shown in Figure 4-6. The apparent mass gain during heating is most probably an artifact caused by an imperfect removal of the instrument response with the test curve that is recorded before the measurement itself. All samples exhibited spallation, which after exposure at 700°C was observed to be initiated after the test period. Data from separate mass measurements are given in Table 4-3.

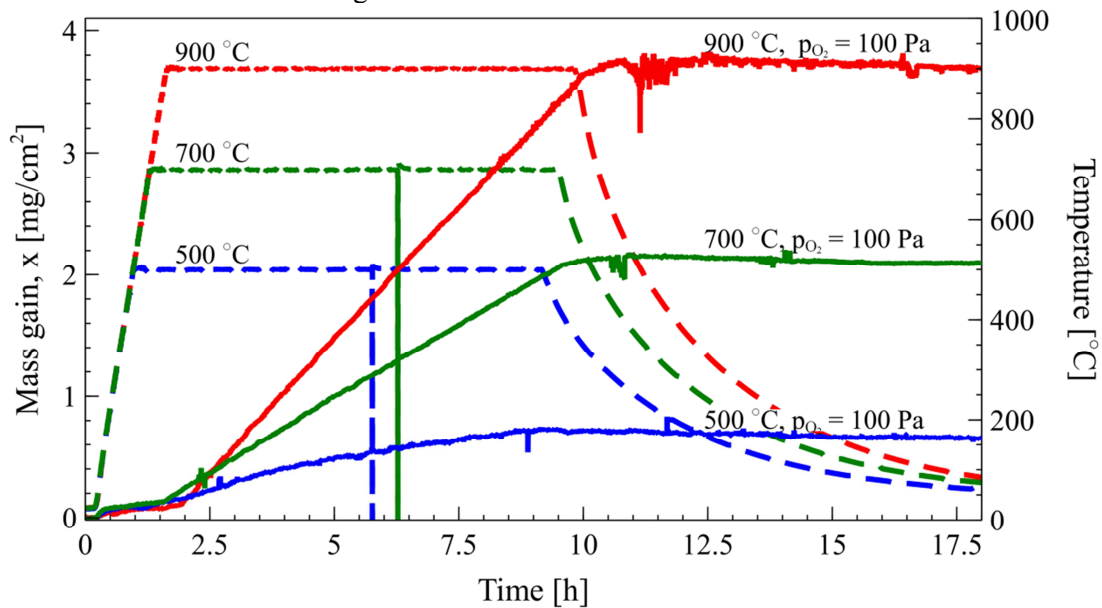


Figure 4-6. Exposure with $p_{O_2} = 100 \text{ Pa}$ (1000 ppm O_2 in Ar) at different temperatures.

Table 4-3. Results from mass measurements before and after exposures with $p_{O_2} = 100 \text{ Pa}$ (1000 ppm O_2 /Ar). In the table, the mass of the sample before exposure, the total weight of sample and crucible before exposure and total weight after exposure are shown. The accuracy of the mass measurements is $60 \mu\text{g}$.

Exposure	Mass of sample before exposure (g)	Total mass of sample and crucible before exposure (g)	Total mass of sample and crucible after exposure (g)	Mass gain (mg)
270°C	4.8757	8.9190	8.9193	0.293
500°C	4.7967	8.8464	8.8497	3.31
700°C	4.8393	8.8888	8.8999	11.04
900°C	4.8876	8.9304	8.9490	18.61

In the exposures with $p_{O_2} = 100 \text{ Pa}$, exposures performed at 700°C and 900°C exhibit a linear behaviour, whereas the data at 500°C differ from the linear behaviour. However, all data could be fitted by eq. 2-2 with results presented in Appendix 1.

4.4 Exposures in Ar/1.8 mol-% H_2 /1000 mol-ppm O_2

After exposure in Ar/1.8 % H_2 /1000 ppm O_2 , the sample exposed at 270°C, displayed a slight discoloration. For the sample exposed at 900°C, the sample was shiny with the milling ridges somewhat less pronounced after exposure and some grain boundaries of the material that could be distinguished by visual inspection (Figure 4-7). Mass gains (Table 4-4) were below the accuracy of the scale, $60 \mu\text{g}$.

The auto-ignition point of hydrogen is approximately 500°C. Above this temperature, the gas environment might also contain some water. If the total amount of oxygen is consumed by hydrogen producing water, the resulting gas environment in the 900°C exposure is Ar/1.6 mol-% H_2 /2000 mol-ppm H_2O . The true composition at 900°C might, depending on the reaction rate of the water reaction, have an oxygen partial pressure between 0 and 100 Pa. As the sample after this exposure seems unaffected, it is possible that the oxygen reacts before reaching the sample.

At 270°C, there is a slight discoloration with no measured mass gain. This might be a sign of oxidation followed by reduction in the exposure or reduction of an existing oxide layer. If the oxide layer is assumed to be homogeneous, the mass gain can be recalculated as oxide thickness using the data $1 \mu\text{g}/\text{cm}^2 = 14.65 \text{ nm}$ (see section 2.4). Based on the accuracy of the scale the change of thickness in the oxide layer has to be below 170 nm. Using the colour of the sample, blue and violet, the thickness can be estimated to about 50 nm (Davis 2001, p 411).

Table 4-4. Results from mass measurements before and after exposures in 90% 2% H_2 /Ar and 10% 1% O_2 /Ar. The accuracy of the mass measurements is 60 μg .

Exposure	Mass of sample before exposure (g)	Total mass of sample and crucible before exposure (g)	Total mass of sample and crucible after exposure (g)	Mass gain (μg)
270°C	4.9043	8.94901	8.94904	30
900°C	4.8906	8.93541	8.93536	-50

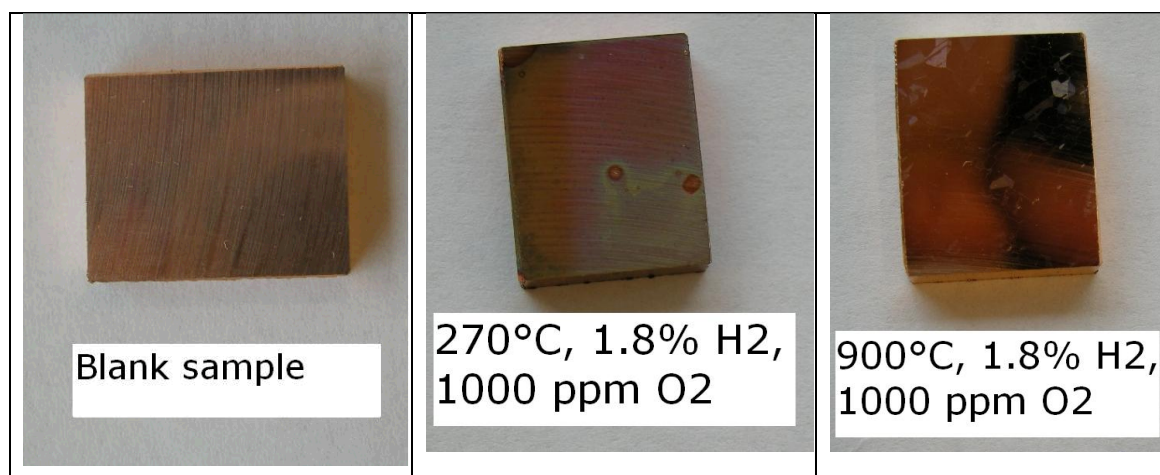


Figure 4-7. Photographs of an unexposed sample and the two samples exposed in 1.8% H_2 /1000 ppm O_2 /Ar.

4.5 Modelling

In order to represent the oxidation kinetics with a mathematical equation mass gain versus time data will be analyzed with the help of equation (2-2). At first an attempt was made to fit the mass gain curves individually and allowing k_p and k_l to vary. The result of that fit showed that the two rate constants were highly coupled and hard to differentiate in some cases. Therefore, the mass gain curves for 900 °C, 700 °C and 500 °C have been fitted to a single model. The data from 270 °C was used as a test for the validity of the model.

The model used for the data is based on equation (2-2), allowing some pre-oxidation of the surface, by introducing a time offset t_0 ,

$$\frac{x}{k_l} + \frac{x^2}{k_p} = t + t_0. \quad (4-1)$$

This is a second degree polynomial with the solution

$$x = \frac{1}{2} \left(-\frac{k_p}{k_l} \pm \sqrt{\left(\frac{k_p}{k_l}\right)^2 + 4k_p(t + t_0)} \right). \quad (4-2)$$

The negative solution can be disregarded since it is not physical with negative mass gains under these circumstances. The value of k_p is taken from the fit of the literature data and the pressure dependence is taken into account as a power law

$$k_p(p_{O_2}, T) = F_p \left(\frac{p_{O_2}}{p_{ref,p}} \right)^{n_p} \left(A_1 e^{-\frac{E_1}{RT}} + A_2 e^{-\frac{E_2}{RT}} \right), \quad (4-3)$$

where n_p is the parabolic power law constant, compare with the power laws given in section 2.3, and $p_{O_2}^{ref,p}$ is the reference oxygen content at which the Arrhenius expression was evaluated, here $p_{O_2}^{ref,p} = 2.1 \times 10^4$. F_p is a scale factor to accommodate changes from the expression gathered from the literature data. In a similar manner the linear rate constant is modelled with

$$k_l(p_{O_2}, T) = A_l \left(\frac{p_{O_2}}{p_{O_2}^{ref,l}} \right)^{n_l} e^{-\frac{E_l}{R} \left(\frac{1}{T} - \frac{1}{T^{ref}} \right)}, \quad (4-4)$$

where A_l is a constant and E_l is the activation energy for the linear rate process, n_l is the power law exponent for the process's pressure dependence, $p_{O_2}^{ref,l}$ is the linear reference pressure, here defined as $p_{O_2}^{ref,l} = 100 \text{ Pa}$, and $T^{ref} = 900^\circ\text{C} = 1173.15^\circ\text{K}$ is a reference temperature.

The above equations were implemented as a model in the GenX fitting software (Björck and Andersson 2007) the resulting parameters that were allowed to be varied can be found in Table 4-5. The time offset was seen to only be important for the parabolic regime and consequently only the data showing a parabolic behaviour was fitted with a time offset. The experiments at 900°C , $p_{O_2} = 2.1 \times 10^4 \text{ Pa}$ and $p_{O_2} = 10^3 \text{ Pa}$ used the same time offset, $t_{0,900^\circ\text{C},21\%1\%}$ and the experiment at 500°C , 1000 ppm used one additional parameter $t_{0,500^\circ\text{C}}$. As the equipment had a background oxygen partial pressure when flushed with pure argon the mean oxygen background pressure, $p_{O_2} = 3.75 \text{ Pa}$, was included as a systematic offset in the model. The resulting agreement of the model with the data can be seen in Figure 4-8. To verify the model's behaviour at lower temperatures as well a comparison with all measured mass gains are presented in Figure 4-9. The maximum deviation between the model and data is 40%. It can be seen that the model shows a systematic underestimation of the amount of oxidation at 270°C .

Table 4-5. The fitting parameters used to refine the model to the data. For the parameters relating to the parabolic behaviour see Table 2-1.

Parameter	Optimized value
A_l	$1.19 \cdot 10^{-7} \text{ g}/(\text{cm}^2\text{s})$
E_l	27 kJ/mol
n_l	1.04
n_p	0.0
$t_{0,900^\circ\text{C},21\%1\%}$	396 s
$t_{0,500^\circ\text{C}}$	308 s
F_p	0.83

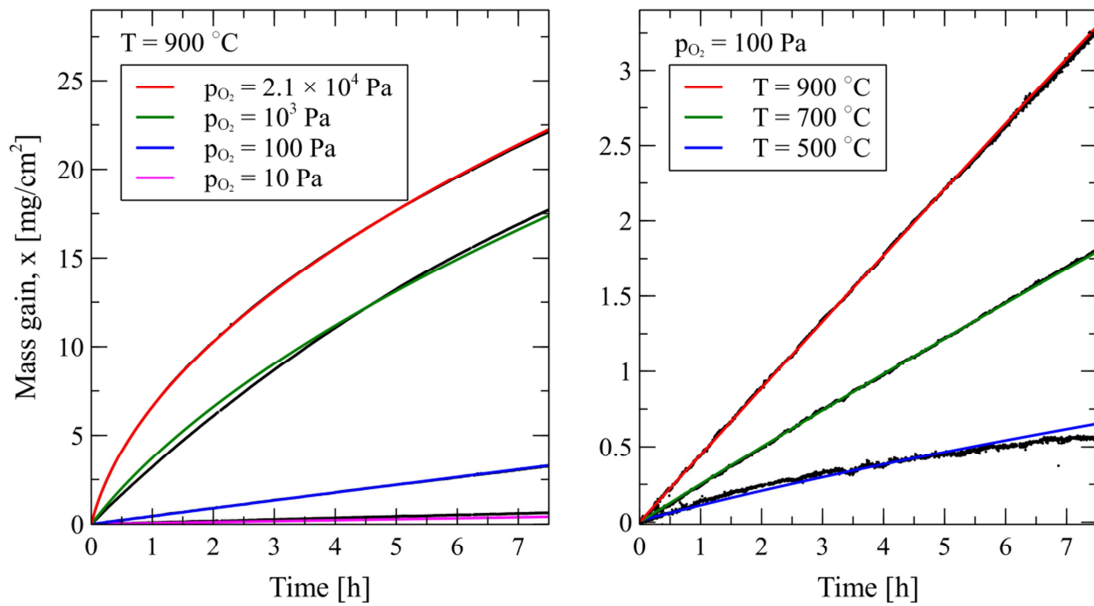


Figure 4-8. The resulting fits of the TGA experiments at **900 °C** with varying oxygen content (left) and for constant oxygen content $p_{O_2} = 100 \text{ Pa}$ with varying temperature. The data is represented by black pixels and identified by the closest fit which is colour coded in the legend.

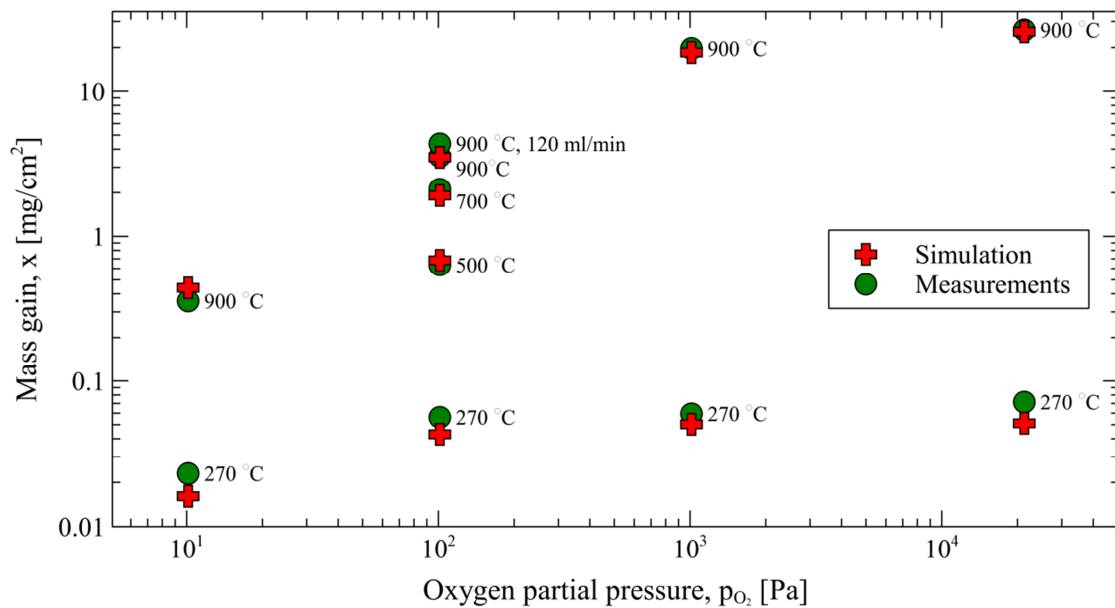


Figure 4-9. The total mass gains as measured by balance for all studied exposures as a function of the oxygen content. The samples exposed at **270 °C** were not included in the fit and serve to validate the model.

The linear oxidation rate constant follows a linear dependence on the O_2 partial pressure. This behaviour is expected if the rate determining step of the reaction is the dissociation of the oxygen molecule on the surface or one of the prior steps in the reaction (Ritchie and Hunt 1969). The activation energy of $27 \text{ kJ/mole} = 0.28 \text{ eV/atom}$ is of the same order of magnitude as the surface self diffusion barrier of oxygen on copper (Korzavyi and Johansson 2011). The fact that the parabolic rate law has no dependence on the oxygen content has not been reported in the literature. Fixing the parabolic exponent to $n_p = 1/7$ yielded a slightly worse fit with a larger $n_l = 1.2$.

The different kinetic regimes can be quantified by the variable $R = 4 \frac{k_l^2}{k_p} (t + t_0)$, see Appendix 2 for a derivation. If $R \gg 1$ a parabolic rate law will prevail and for $R \ll 1$ linear kinetics will dominate. As $t \rightarrow \infty$ transport through the copper oxide layer must dominate and consequently parabolic kinetics will result, which agrees with the expression for R . In order to observe the different regimes, a phase diagram of the kinetics regimes as a function of the temperature and oxygen pressure using the fitted parameters in Table 4-5 is shown in Figure 4-10. The different kinetic regimes can be compared to the data in Appendix 1 where it can be seen that the different regimes correspond to the transition in Figure 4-10. At 900°C the transition starts at $p_{O_2} = 10^3$ Pa and is completely linear at $p_{O_2} = 100$ Pa. For the data collected at $p_{O_2} = 100$ Pa the curves are linear for 900°C and 700°C but the curve for 500°C shows some parabolic behaviour. This is in agreement with Figure 4-10. Also the 270°C data does not show a change in its mass gain, see Figure 4-9, until it has transcended into the linear regime.

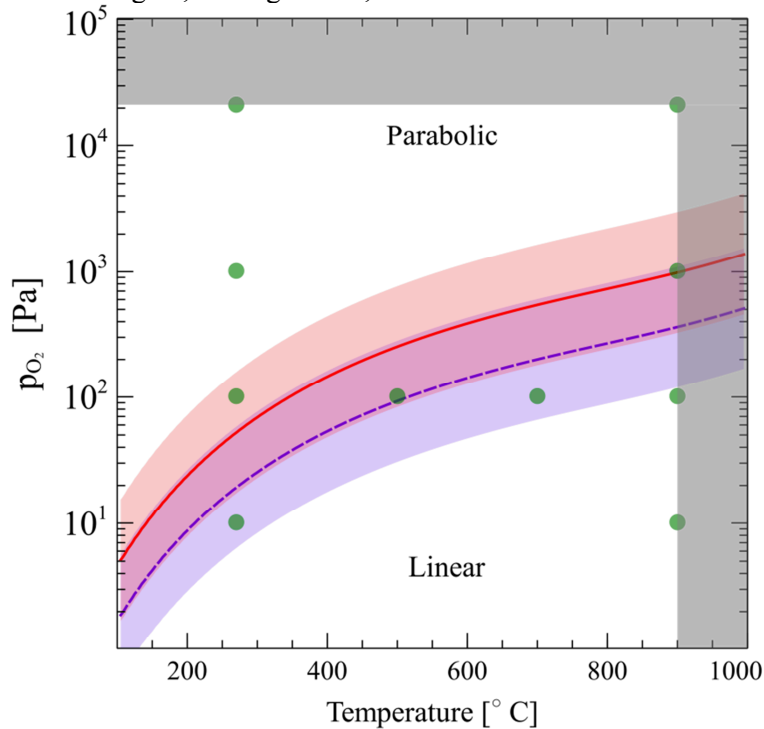


Figure 4-10. The dominating rate law as a function of the oxygen content and temperature. The red full line denotes the boundary, $R = 1$, between the parabolic and linear regimes with the filled semitransparent red transition area, $0.1 \leq R \leq 10$, for a time $t = 1$ h. The blue dotted line with an accompanying blue semi transparent area shows the equivalent quantities for $t = 8$ h. The green circles denote the experiments conducted in this study. The grey area in the graph is parameter combinations expected to lie outside the FSW process.

The model presented has been validated in the range 900 °C to 270°C and at oxygen partial pressures down to $p_{O_2} = 10$ Pa. However, oxidation only ceases at temperatures below 100°C at $p_{O_2} = 2.1 \times 10^4$ Pa. There is a temperature region of 170 °C that has not been validated. In this region it is not possible to do experiments using the equipment utilised in this study. Some estimates of the validity of the model can anyway be drawn. Firstly, the parabolic regime will dominate down to at least the same p_{O_2} as for 270 °C, which implies that the model has been validated indirectly, by comparison to literature data, down to between $p_{O_2} = 10$ Pa and $p_{O_2} = 100$ Pa. Secondly, doing a linear extrapolation of the maximum relative error for the 270 °C data, 40 %, to a temperature of 170 °C and assuming that the error is zero at 500°C yields an maximum error of 70%.

5 Conclusions

A model for the oxidation kinetics of copper at reduced oxygen partial pressures in an inert gas atmosphere has been developed based on previous work in the literature as well as new experimental work to complement and extend the previous studies. Based on a literature survey it was found that the oxidation kinetics of copper has been little studied at oxygen partial pressures below 10^3 Pa. The experimental work, using TGA measurements, was focused in the temperature range 270 °C to 900°C and oxygen partial pressures in the range 2.1×10^4 Pa to 10 Pa. The higher oxygen contents were included in order to verify the new experiments against previous work.

The experiments showed a parabolic regime at high oxygen contents and a linear regime at lower oxygen contents, in qualitative agreement with previous literature data. A model based on a competing linear, a surface reaction limited, and parabolic, diffusive transport limited, regime was fitted to part of the data. Literature data was used to refine the temperature dependence of the parabolic part of the model. The low temperature data was used to validate the model. A maximum deviation of 40% between the model and experimental data was found at low temperature.

As a comparison two exposures in a hydrogen containing atmosphere (Ar/1.8 mol-% H₂/1000 mol-ppm O₂) with a maximum oxygen partial pressure of 100 Pa were done in order to evaluate the effect of a reducing atmosphere. All samples showed a weight increase below the accuracy of the scale, 60 μ g, which is one order of magnitude lower than any other exposure done in this study.

References

SKB's (Svensk Kärnbränslehantering AB) publications can be found at www.skb.se/publications.
References to SKB's unpublished documents are listed separately at the end of the reference list.
Unpublished documents will be submitted upon request to document@skb.se.

- Andersson H C M, Seitisleam F, Sandström R, 2007.** Creep testing and creep loading experiments on friction stir welds in copper at 75 °C. SKB TR-07-08, Svensk Kärnbränslehantering AB.
- Andersson-Östling H C M, Sandström R, 2009.** Survey of creep properties of copper intended for nuclear waste disposal. SKB TR-09-32, Svensk Kärnbränslehantering AB.
- Auerkari P, Rantala J, Salonen J, Laukkanen A, Holmström S, Kinnunen T, 2012.** Effect of defects on low temperature creep of OFP copper. In Shibli I A, Holdsworth S R (eds). Creep & fracture in high temperature components: design & life assessment issues: proceedings of the 2nd ECCO Creep Conference, Zürich, 21–23 April 2009. Lancaster, PA: DEStech Publications, 287–297.
- Björck M, Andersson G, 2007.** GenX: an extensible X-ray reflectivity refinement program utilizing differential evolution. *Journal of Applied Crystallography* 40, 1174–1178.
- Cabrera N, Mott N F, 1949.** Theory of the oxidation of metals. *Reports on Progress in Physics* 12, 163–184.
- Davis J R (ed), 2001.** Copper and copper alloys. Materials Park OH: ASM International. (ASM speciality handbook)
- Deal B E, Grove A S, 1965.** General relationship for the thermal oxidation of silicon. *Journal of Applied Physics* 36, 3770–3778.
- Gubner R, Andersson U, 2007.** Corrosion resistance of copper canister weld material. SKB TR-07-07, Svensk Kärnbränslehantering AB.
- Iijima J, Lim J-W, Hong S-H, Suzuki S, Mimura K, Isshiki M, 2006.** Native oxidation of ultra high purity Cu bulk and thin films. *Applied Surface Science*, 253, 2825–2829.
- Kofstad P, 1988.** High temperature corrosion. London: Elsevier Applied Science.
- Korzhavyi P A, Johansson B, 2011.** Literature review on the properties of cuprous oxide Cu₂O and the process of copper oxidation. SKB TR-11-08, Svensk Kärnbränslehantering AB.
- Krishnamoorthy P K, Sircar S C, 1970.** Formation of very thin oxide films on copper: kinetics and mechanism. *Oxidation of Metals* 2, 349–360.
- Mrowec S, Stoklosa A, 1971.** Oxidation of copper at high temperatures. *Oxidation of Metals* 3, 291–311.
- Ogbuji L, Humphrey D L, 2003.** Comparison of the oxidation rates of some new copper alloys. *Oxidation of Metals* 60, 271–291.
- Pinnel M R, Tompkins H G, Heath D E, 1979.** Oxidation of copper in controlled clean air and standard laboratory air at 50 °C to 150 °C. *Applications of Surface Science* 2, 558–577.
- Rauh M, Wißmann P, 1993.** The oxidation kinetics of thin copper films studied by ellipsometry. *Thin Solid Films* 228, 121–124.

Rice D, Peterson P, Rigby E, Phipps P, 1981. Atmospheric corrosion of copper and silver. Journal of the Electrochemical Society, 128, 275–284.

Ritchie I M, Hunt G L, 1969. The kinetics and pressure dependence of surface controlled metal oxidation reactions. Surface Science 15, 524–534.

Ronneteg U, Cederqvist L, Rydén H, Öberg T, Müller C, 2006. Reliability in sealing of canister for spent nuclear fuel. SKB R-06-26, Svensk Kärnbränslehantering AB.

Roy S K, Bose S K, Sircar S C, 1991. Pressure dependencies of copper oxidation for low-and high-temperature parabolic laws. Oxidation of Metals 35, 1–18.

Rönqvist A, Fischmeister H, 1961. The oxidation of copper – a review of published data. Journal of the Institute of Metals 89, 65–76.

Savolainen K, 2012. Friction stir welding of copper and microstructure and properties of the welds. PhD thesis. Aalto University, Espoo, Finland.

SKB, 2010. Design, production and initial state of the canister. SKB TR-10-14, Svensk Kärnbränslehantering AB.

Suzuki S, Ishikawa Y, Isshiki M, 1997. Native oxide layers formed on the surface of ultra high-purity iron and copper investigated by angle resolved XPS. Materials transactions, JIM 38, 1004-1009.

Wagner C, Grünwald K, 1938. Beitrag zur Theorie des Anlaufvorganges. Zeitschrift für Physikalische Chemie B, 455–475.

Zhu Y, Mimura K, Lim J-W, Isshiki M, Jiang Q, 2006. Brief review of oxidation kinetics of copper at 350 °C to 1050 °C. Metallurgical and Materials Transactions A 37, 1231–1237.

Yang J C, Kolasa B, Gibson J M, Yeadon M, 1998. Self-limiting oxidation of copper. Applied Physics Letters 73, 2841.

Unpublished documents

SKBdoc id, version	Title	Issuer, year
1371191 ver 1.0	FSWL94 – Measurement of temperatures and surrounding oxygen levels during welding	SKB, 2013

Appendix 1

The figure shows all TGA data fitted to the three models discussed in the report. It shows that the combined model, eq. (2-2), provide a more accurate fit than the linear and parabolic rate laws.

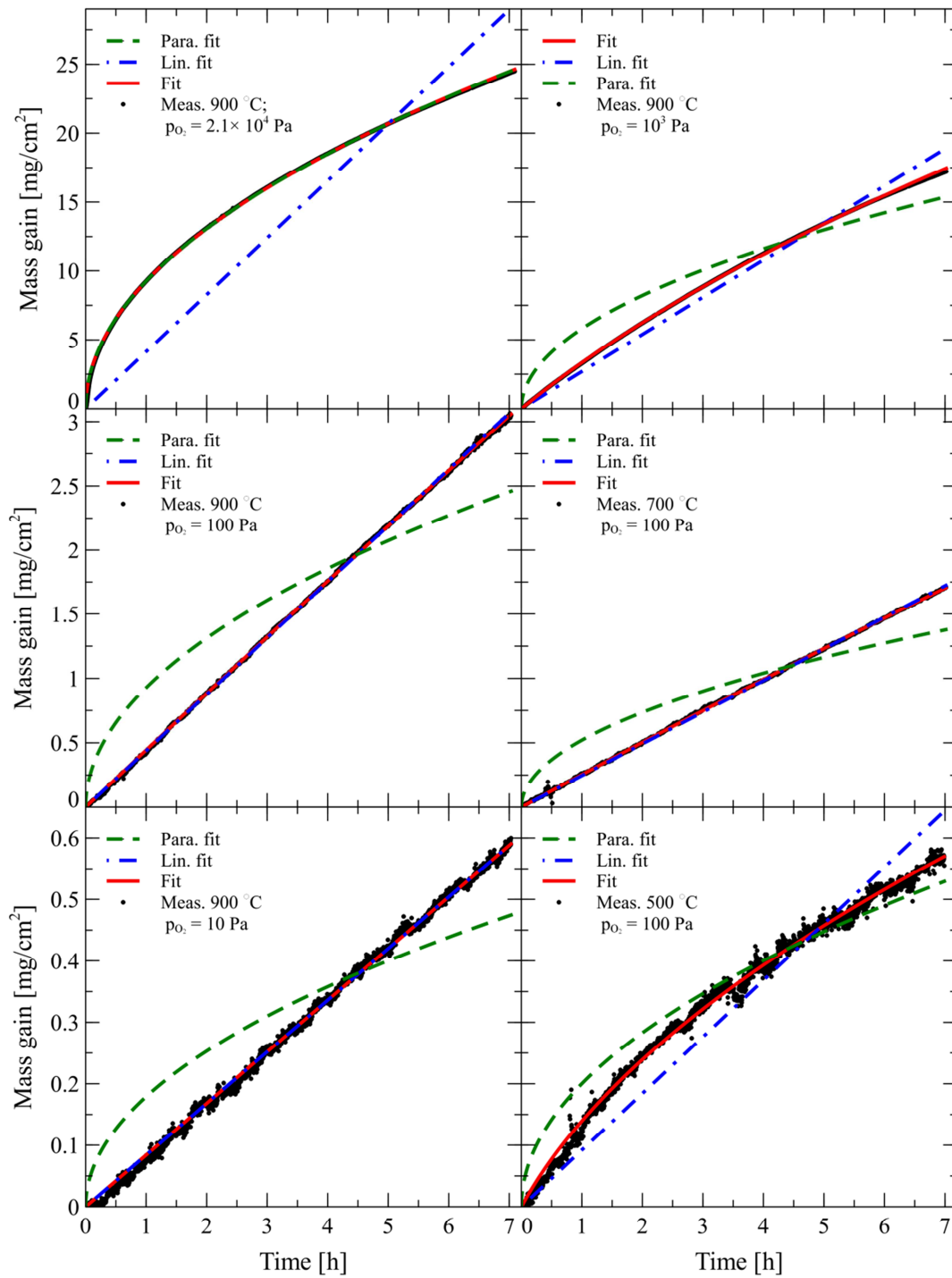


Figure 0-1. Collection of all TGA data with fits to the model (eq. (2-2)) included to show the applicability of the model.

Appendix 2

In order to quantify the transition from a completely parabolic regime to a completely linear regime a state parameter can be defined by observing the limiting cases of equation (2-2). Equation (2-2) can be rewritten as

$$x = \frac{1}{2} \frac{k_p}{k_l} \left(-1 + \sqrt{1 + 4 \frac{k_l^2}{k_p} (t + t_0)} \right). \quad (0-1)$$

If $4 \frac{k_l^2}{k_p} (t + t_0) \ll 1$ the expression under the root sign can be Taylor expanded to yield

$$\sqrt{1 + \frac{k_l^2}{k_p} (t + t_0)} \approx 1 + \frac{1}{2} \frac{k_l^2}{k_p} (t + t_0), \quad (0-2)$$

which results in that equation (0-1) simplifies into

$$x \approx k_l (t + t_0). \quad (0-3)$$

This is a linear rate law. The other extreme is when $4 \frac{k_l^2}{k_p} (t + t_0) \gg 1$. Then equation (0-1) simplifies into

$$x \approx \frac{1}{2} \frac{k_p}{k_l} \left(-1 + \sqrt{4 \frac{k_l^2}{k_p} (t + t_0)} \right) \approx \sqrt{k_p (t + t_0)} - \frac{1}{2} \frac{k_p}{k_l}, \quad (0-4)$$

which is a parabolic rate law.

Given the above considerations the quantity $R = 4 \frac{k_l^2}{k_p} (t + t_0)$ describes the continuous change between a parabolic rate law, $R \gg 1$, and a linear law, $R \ll 1$.